INTERNATIONAL JOURNAL FOR NUMERICAL METHODS IN FLUIDS
*Int. J. Numer. Meth. Fluids* 2003; **43**:637–650 (DOI: 10.1002/fld.544)

# Applications of patient-specific CFD in medicine and life sciences

Rainald Löhner[1,*,†], Juan Cebral[1], Orlando Soto[1], Peter Yim[2] and James E. Burgess[3]

[1]*School of Computational Sciences, M.S. 4C7, George Mason University, Fairfax, VA 22030-4444, U.S.A.*
[2]*Diagnostic Radiology Department, National Institutes of Health, Bethesda, MD, U.S.A.*
[3]*Neurosurgery, INOVA, Fairfax Hospital, Fairfax, Virginia, U.S.A.*

SUMMARY

Recent advances in medical image segmentation, grid generation, flow solvers, realistic boundary conditions, fluid–structure interaction, data reduction and visualization arc reviewed with special emphasis on patient-specific flow prediction. At the same time, present shortcomings in each one of these areas are identified. Several examples are given that show that this methodology is maturing rapidly, and may soon find widespread use in medicine. Copyright © 2003 John Wiley & Sons, Ltd.

KEY WORDS: hemodynamics; pulmonary flows; CFD; bioengineering

## 1. INTRODUCTION

The vascular system (arteries and veins) delivers nutrients and retrieves waste products. The respiratory system delivers oxygen and retrieves carbon dyoxide. These vital transport systems are mainly tubular in nature, and are powered by the heart and lung, respectively. Any kind of damage or obstruction of these transport systems will, in all likelihood, result in a variety of diseases than can have a profound effect on wellness and quality of life. Vessel damage or obstruction may be treated by a variety of surgical and interventional procedures: stenting, balloon angioplasty, *in situ* drug delivery for unclotting, bypass surgery, artificial organ implantation, etc. Many of these procedures are performed daily on thousands of patients, and have led to an impressive empirical knowledge database. Some of these

* Correspondence to: R. Löhner, School of Computational Sciences, M.S. 4C7, George Mason University, Fairfax, VA 22030-4444, U.S.A.
† E-mail: rlohner@gmu.edu

Contract/grant sponsor: AFOSR, Whitaker Foundation


*Received 3 March 2002*
*Revised 19 February 2003*

procedures have statistically significant failure rates, indicating a need to study in depth the fluid dynamics before and after the intervention. As in the manufacturing industries, it would be highly desirable to predict the outcome of an intervention before 'cutting tissue', particularly for complex cases where a detailed empirical database is lacking.

The basic steps required for any type of flow simulation are the following:

- Pre-processing or problem definition:
  - Geometry (surface);
  - Boundary and initial conditions;
- Grid generation;
- Fluid–structure solver and
- Visualization and data deduction.

Any type of interventional simulation will require accurate modelling of patient-specific anatomy and physiologic conditions. It is here where the biggest obstacle to routine simulations lies. Typically, only the anatomy is imaged. Flows may be measured non-invasively by phase-contrast magnetic resonance (PCMR) or Doppler ultrasound (US). However, the accuracy for these measurements can be problematic due to imaging artifacts and noise. The compliance of an arterial wall is difficult to obtain, and its pressure/diameter relation may be highly non-linear. Nevertheless, recent advances in:

- Radiology (high contrast imaging);
- Image-to-surface definition tools;
- Automatic grid generation;
- Fast incompressible flow solvers and realistic boundary conditions;
- Fluid–structure interaction techniques;
- Insightful visualization;
- Validation in the form of *in vitro*/*vivo* studies; and
- Increased compute and graphics power.

have led to a favourable confluence of techniques that have made predictions on the living human being possible, and in some cases, routinely so.

In the sequel, we focus on recent advances, outstanding issues and obstacles for each one of these areas. Thereafter, we show several examples to demonstrate that what was a vision several years ago is maturing rapidly and may indeed lead to clinical tools in the near future.

## 2. IMAGE-TO-SURFACE DEFINITION TOOLS

The starting point for most non-invasive patient-specific simulations is an image, i.e. an array of pixels with different colours. Imaging modalities currently in use are: digital subtraction angiography (DSA), magnetic resonance angiography (MRA), computed tomography (CT), and xenon-CT (XeCT). The overall quality (sharpness) of medical images depends not only on hardware factors (resolution, wavelength, etc.), but also on type of contrast agent used, the skill of the radiologist and patient-specific factors. This implies that in many cases, medical images will exhibit coarse resolution and noise, i.e. require considerable experience and/or 'guessing' to be interpreted correctly. In order to conduct any kind of flow simulation for the some or all of the vessels present in the imaged region, the surface of these vessels needs to

 

be extracted. Numerous techniques have been explored over the last decade, of which we list a few here:

*Active contours*: This most common approach consists in 2D image segmentation based on edge detection, followed by slice interpolation, stacking and meshing [1–4]. Although there are many contour and edge detection operators, there is still no algorithm that can automatically extract region boundaries perfectly from medical images [5]. Besides, this technique requires a large amount of manual input, and does not work properly for situations where the vessel is not perpendicular to the image slices (e.g. complex bifurcations and aneurysms).

*Deformable models*: In this case, an initial, given shape is iteratively deformed by solving an equivalent elastic problem driven by the image intensity gradient [6–8]. The major drawback is that the initial shape (or skeleton) must have the same topology as the reconstructed boundary. For simple vessels and bifurcations this is perhaps the best technique available. However, patient-specific simulations with complex geometries are difficult, and in many instances this technique requires substantial human intervention, making the whole process tedious and time consuming.

*Skeletonization and deformable models*: These techniques assume that the surfaces to be extracted are of tubular nature, i.e. have a skeleton of centrelines [9, 10]. In a first step, these centrelines are extracted from the image. In a second step, the thickness of the vessels is obtained by 'inflating' the centrelines in order to match the vessel boundaries. In some cases, each individual vessel is obtained separately, so that the complete vessel tree is obtained in a third step that joins the separate branches. The end result is a triangulation that defines the vessel geometry. The amount of manual 'guidance' varies from technique to technique, but can be considerable for some. This type of technique works very well for tubular structures, i.e. for most of the vascular system. However, it will not work well for regions where centrelines are not well defined, such are highly stenosed vessels or aneurysms.

*Region growing with isosurface extraction*: These techniques interpret the pixels of the image as a mesh, i.e. with an undelying point and element structure. Given the local distribution of pixel intensity, an iso-surface of constant value can be obtained. The regions covered by the vessels of interest are obtained using region growing algorithms [11–19]. Starting from one or more the so-called seedpoints, all the voxels falling into the region of interest (typically given by an intensity threshold) are queried for a given intensity value. The iso-surface obtained in this way is given as a triangulation.

None of the techniques outlined above is, at this point, universally applicable. In particular, images that exhibit vessels in close proximity can lead to wrong vessel interpretation. The automatic reconstruction of arterial trees involving several arterial generations also constitutes an unsolved problem. Perhaps a combination of different techniques for different entities (e.g. vessels, aneurysms, etc.) will lead to new breakthroughs.

The triangulation extracted from the medical image at hand, no matter which technique is being used, must be post-processed further. We mention:

(a) *Surface improvement*: Depending on the vessel surface extraction technique used the triangulations obtained can contain:

- Elements that have extremely large or small angles;
- Small elements surrounded by much larger elements and
- Elements with large normal jumps between neighbours.

 

These elements are removed using edge or element collapse, as well as diagonal swapping [15–21].

(b) *Surface smoothing*: Depending on the vessel surface extraction technique used and the image resolution, the triangulations obtained will exhibit bumps, sharp corners or other anormalities that are not present in the actual vessel. This implies that a surface smoothing step is required. A number of surface smoothing techniques have appeared in the literature. We have used the non-shrinking smoothing of Taubin [22].

(c) *Branch cutting*: Vessels tend to become smaller and smaller as one progresses along the arterial tree. At some point, geometry resolution or flux resolution is insufficient, and a boundary condition has to be applied to limit the computational domain. This implies that a branch cutting tool has to be devised. Many techniques arc possible. We have used iso-distance contours to cut branches interactively [15–19].

(d) *Construction of post-operational models*: Given the pre-operational anatomy, and the expected modification (e.g. due to stenting or bypass surgery), the post-operational model can be constructed. This will involve surface merging, cutting, blending, etc. We have used iso-surface-based techniques to perform such operations in an expedient way [23, 24].

## 3. AUTOMATIC GRID GENERATION

Any field solver requires some form of volume discretization. Given their high degree of flexibility and automation, unstructured grids based on tetrahedra have been almost universally adopted for patient-specific vessel simulations. Recent advances in:

- Discrete surface gridding and
- Minimal input grid generation

have enabled fully automatic grid generation of highly complex arterial and bronchial geometries [17–19]. We mention a few of these advances in the sequel, as well as outstanding issues for further investigation.

(a) *Discrete surface gridding*: The vessel geometry is not defined as an analytical surface patch, but as a triangulation. This implies that robust automatic surface triangulation techniques that operate on discrete surface patches have to be devised. For a number of years, we have used an advancing front technique on these discrete surface patches [25, 26]. Recent improvements include: automatic preprocessing/improvement of the given discrete surface patch grid, the definition and enforcement of the so-called sharp edges, a strict enforcement of continuous topology, and improved front-crossing checks [27, 28].

(b) *Minimal input grid generation*: The definition of proper element size and shape for arterial or bronchial trees with several branching generations can be a tedious, time-consuming process. In order to alleviate this problem, we have used adaptive background grids based on the local discrete surface patch curvature [27, 28]. This leads to grids where the number of elements per vessel diameter is always sufficient, without generating too many elements in the larger vessels.

As an outstanding research topic we mention the automatic generation of optimal grids for tubular structures. The idea here is to generate stretched elements along the main direction of a vessel. This technique could potentially reduce the number of elements and CPU time requirements by a factor of 1:5.

 

## 4. FAST INCOMPRESSIBLE FLOW SOLVERS

The equations describing incompressible flows may be written as

$$\mathbf{v}_{,t} + \mathbf{v}\nabla\mathbf{v} + \nabla p = \nabla\mu\nabla\mathbf{v} \tag{1}$$

$$\nabla \cdot \mathbf{v} = 0 \tag{2}$$

Here $p$ denotes the pressure, $\mathbf{v}$ the velocity vector and both the pressure $p$ and the viscosity $\mu$ have been normalized by the (constant) density $\rho$. Blood is a non-Newtonian fluid, implying that the viscosity $\mu$ depends on the strain rate tensor. The last two decades have seen impressive progress in our ability to solve these equations in an expedient manner. Key elements of any modern incompressible flow solver include:

- An arbitrary Lagrangean–Eulerian (ALE) formulation for moving walls (deforming grids);
- Implicit timestepping;
- Some form of upwinding with limiters for the advection operator;
- Satisfaction of the LBB condition for the divergence constraint, either via mixed elements [29, 30], artificial dissipation [31–33] or consistent numerical fluxes [34],
- Preconditioned iterative solvers [35–38] for all large systems of equations that require inversion;
- Edge-based data structures for reduced indirect addressing and optimal operation count [39, 28]; and
- Minimal cache misses, vectorization and parallelization options [40].

Further algorithmic gains may come from the use of LU-SGS preconditioning [41, 42] and multigrid [43, 44]. We have not seen the use of these techniques for medical flow applications, but see no reason why the success they have had in other fields can not be duplicated here as well.

*Boundary conditions*: The imposition of proper flow boundary conditions represents one of the most difficult, and admittedly questionable, aspects of patient-specific simulations. In the first place, the flux data is not easy to obtain. Measuring velocity profiles via phase-contrast MR (PCMR) requires non-standard imaging protocols and a longer scanning time. Then there is the question of resolution. The number of pixels required for accurate vessel geometry reconstruction is much lower than the number of pixels required for accurate flow profile reconstruction. Only the velocity normal to the MR cut is measured, i.e. a complete characterization of the velocity field would require even longer scanning times. For this reason only the velocity normal to a cut is measured, i.e. all cross-velocity information is lost. For some vessels, peak velocities can be measured using ultrasound techniques, and these can in turn be used to impose boundary conditions. On the other hand, we know that the flow in curved tubular structures can exhibit considerable cross flow, and that any form of cross flow can have significant effects downstream.

To date, most CFD simulations have been carried out prescribing fully developed, time-dependent velocity profiles derived from flow-rate curves using the Womersley solution [45]. The Womersley solution holds only for pulsating flow in an infinitely long circular cylinder. For other vessel cross-sections the Womersley profiles are mapped accordingly.

 

Pressure boundary conditions are important for fluid–structure interactions simulations with compliant walls. Pressures can be obtained invasively using catheters, but it would be highly desirable to develop non-invasive pressure measuring techniques.

Major outstanding problems in this field are:

(a) The derivation of post-operative boundary conditions from pre-operative data [55, 23, 24]; and
(b) The derivation of boundary conditions when complete information is unavailable. A typical case is the Circle of Willis. We do not expect to be able to obtain complete flow and pressure data for this complex arterial system for years to come. Examples of work in this area include vascular bed models [17–19] and the link of detailed 3D models with 1D models of the whole cardiovascular system [2].

## 5. STRUCTURAL DEFORMATION MODELS

Arterial wall movement may have a profound effect on local flow conditions. One observes that fluxes do not 'add up' if the deformation of the wall is neglected. In principle, the vessel wall and the surrounding medium can be modelled using a structural dynamics solver for 3D non-linear, large-deformation behaviour. However, the difficulties in obtaining proper initial and boundary conditions are even more pronounced here than for the flow solver. The material is highly non-linear, orthotropic, layered, may be responding, etc. How to obtain this information non-invasively is, at this point, an open question. For this reason, most wall deformations have been computed using shells [46, 47] or, even simpler, an independent ring model [2]. In this case, the normal wall displacement $\eta$ is obtained from:

$$m\eta_{,tt} + d\eta_{,t} + k\eta = p, \quad m = \rho_w h, \quad k = \frac{Eh}{(1-\nu^2)r^2} \tag{3}$$

where $\rho_w, h, r, E, \nu$ denote, respectively, the wall density, thickness, vessel radius, Young's modulus and Poisson's ratio. This equation is integrated using a second-order implicit time integration scheme. As stated before, measuring $h, r, E, \nu$ is no simple matter [47, 48].

## 6. FLUID–STRUCTURE INTERACTION TECHNIQUES

Given that vessel deformation plays an important role for local flux evaluations, the fluid and structure models must be combined. Due to their generality, modularity and extendability the so-called loose coupling techniques have been used extensively in engineering (see, e.g. [49]). The key idea is to have a master code that invokes the fluid and structural codes alternatively in such a way that a minimum of changes are required for the latter. All data transfer is handled by a separate library. We remark that this is not only a matter of fast interpolation techniques [50, 51], but also of accuracy, load conservation [52, 53], geometrical fidelity [52, 53] and temporal synchronization [52–54]. For implicit CFD and CSD codes, we

 

use the following underrelaxed predictor-corrector scheme for each timestep:

```
while: not converged:
    update structure with fluid loads:
        x_s^i = (1 − α) x_s^{i−1} + α f(σ_f^i)
    update fluid with structure position/velocity:
        σ_f^i = (1 − α) σ_f^{i−1} + α g(x_s^i)
endwhile
```

Typical underrelaxation factors are in the range $0.5 \leqslant \alpha \leqslant 0.9$. Current research in this area is focused on convergence criteria and acceleration techniques.

## 7. INSIGHTFUL VISUALIZATION

In order to enhance the understanding and prediction capability of patient-specific simulations, the results obtained must be presented in a form easily accessible to the medical community. In the particular case of tubular structures, many classic visualization techniques fail to offer insight. This is because iso-surfaces or plane cut, staples in the engineering world, become meaningless. A plane cut through a twisted, winding arterial or bronchial tree will lead to a few scattered ellipsoids here and there that offer no insight on fluxes, pressures, etc. For this reason, we have developed specialized reduction techniques [23, 24] that work with the skeleton of the tubular structure in order to display:

- Plane cuts normal to the skeleton;
- Plane cuts along the skeleton;
- Fluxes along the skeleton;
- Iso-distance to wall surfaces, etc.

These reduction techniques have proven extremely beneficial in identifying important flow features such as local recirculation zones and flow rates. Other techniques that have found widespread use in computational hemodynamics include particle tracking (where there is an immediate mental connection to blood cells) and the use of transport equations to observe the dispersion of tracers.

## 8. VALIDATION

In order to validate at least partially the methodology developed to date, a phantom glass model of a cartid bifurcation with 65% stenosis in the internal carotid artery was measured and computed. The model, as well as the cuts used for MRA flow measurements are shown in Figure 1(a). The CFD model was generated from the MRA data. The discrepancy in the radii obtained from image processing and segmentation was less than 2%. Parabolic velocity profiles based on measured fluxes were prescribed at the entrance and exit of the external carotid. Figure 1(b) shows a comparison of the absolute value of the velocities (CFD) and the normal velocity measured (MRA) for the cuts labelled A–A, B–B, in Figure 1(a). One can clearly see how coarse the resolution of the MRA is. Figure 1(c) shows the absolute value of the velocity in the centreplane and the streamlines. Note the large recirculation zone present.

 

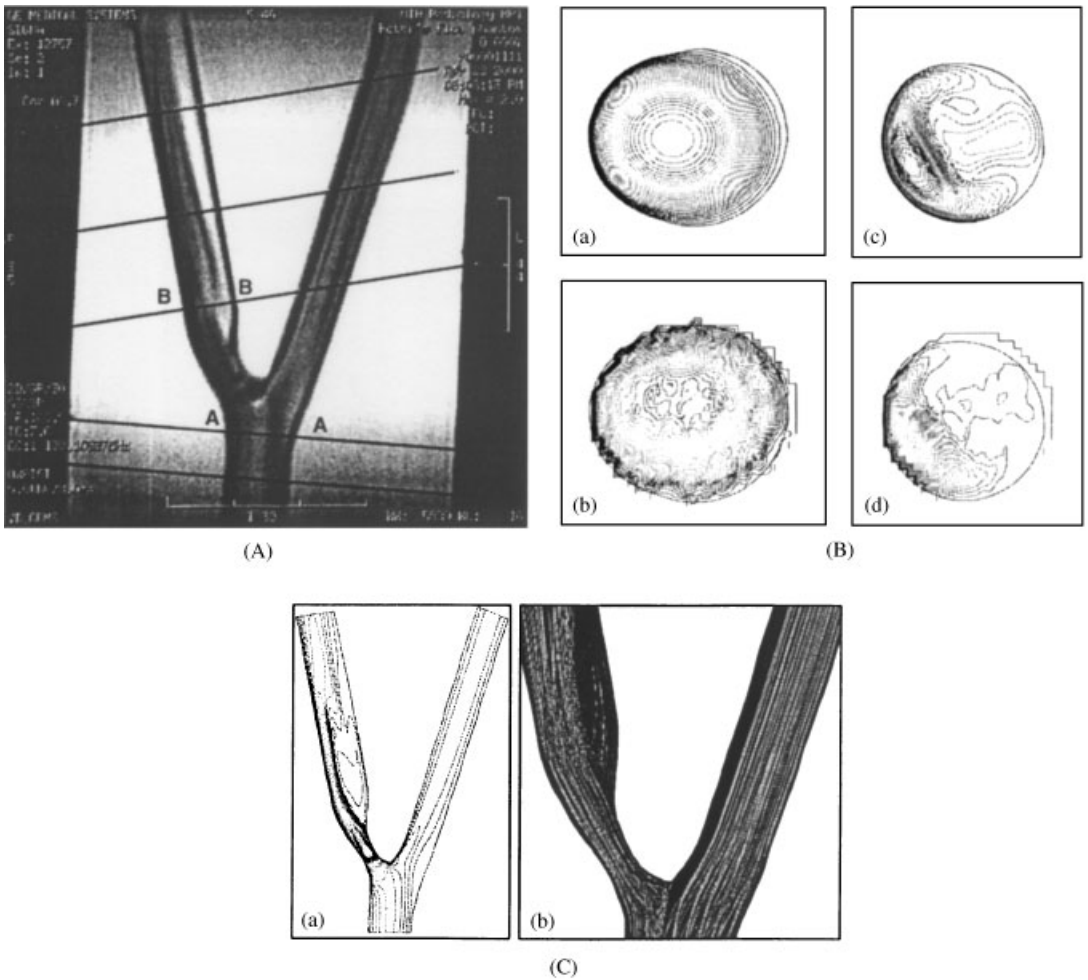


Figure 1. (a) Phantom: MIP geometry definition and MRA cuts. (b) Phantom: comparison of velocities (CFD-MRA). (c) Phantom: abs(Vel) in plane and streamlines.

## 9. EXAMPLES

E.1 *Circle of Willis*: The aim of this simulation was to assess the effect of clipping an artery in the Circle of Willis on the overall flow pattern. Figure 2(a) shows the graphical interface used for image processing, segmentation, surface extraction and surface improvement. One can clearly discern the maximum intensity projection (MIP) on the upper left side, as well as two other cuts and the main 3D window with the extracted and cut surface. The surface mesh is shown in Figure 2(b). The volume mesh had approximately 4 million tetrahedra. Figure 2(c) shows streamribbons for an unclipped (left) and clipped (right) artery superposed on the volume rendered anatomy. These views show

 

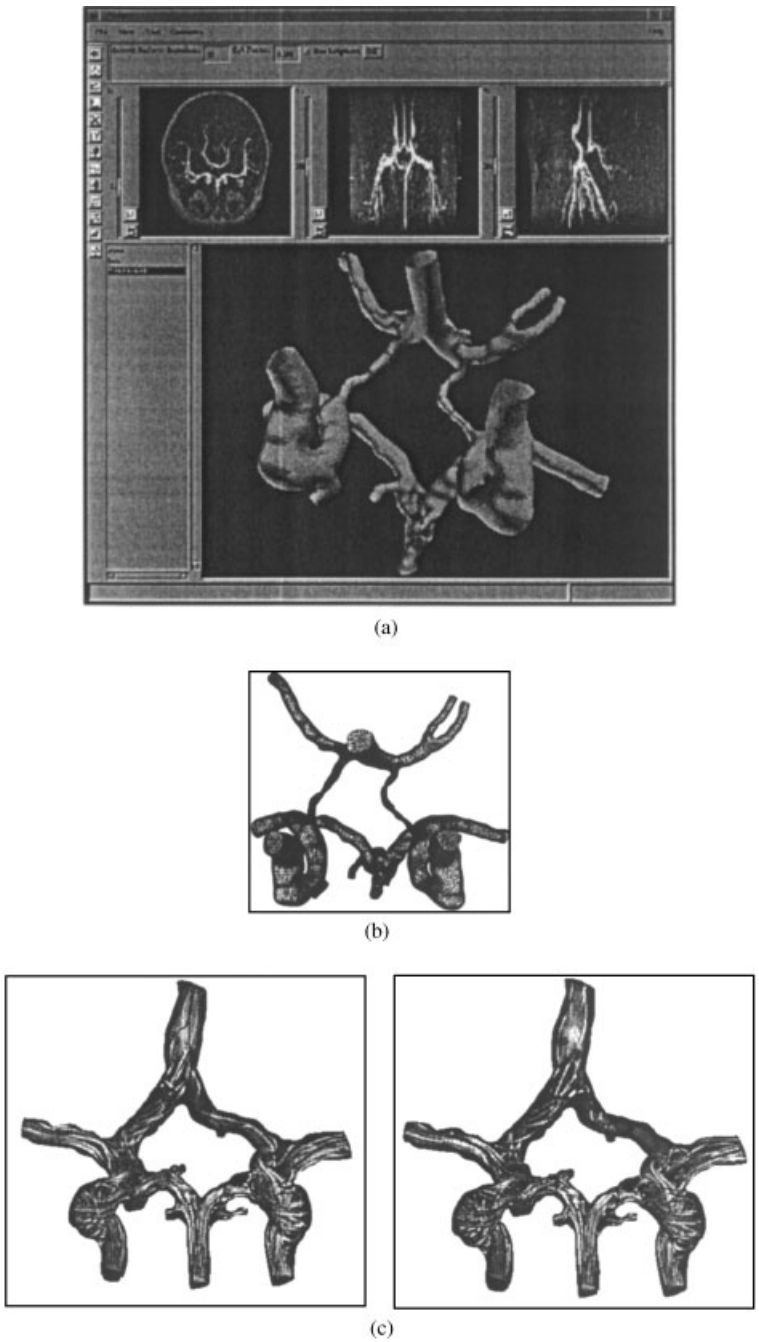

Figure 2. (a) Circle of Willis: Zhemo user interface. (b) Circle of Willis: surface mesh. (c) Circle of Willis: Streamribbons for open and clipped cases.

 

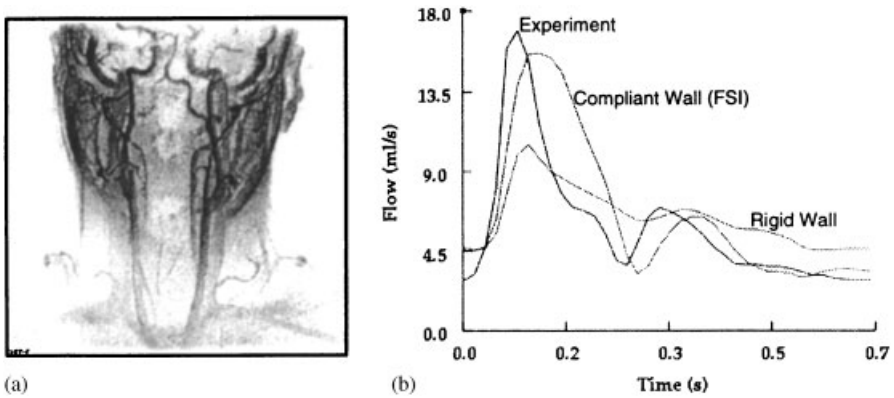


Figure 3. (a, b) Carotid bifurcation: MIP and comparison of fluxes.

how CFD can be used to complement current anatomy-based diagnostics for surgical planning.

E.2 *Carotid bifurcation*: This case shows the need to couple fluid and structural codes to predict arterial flows. The anatomical data was taken from a normal human subject. A model of the right carotid artery of the subject was reconstructed from contrast-enhanced MRA images. Figure 3(a) shows the maximum intensity projection (MIP) of the anatomical images. Four 2D phase-contrast MRA images were taken at different locations, two along the common carotid artery (CCA) below bifurcation, and two above the bifurcation. Figure 3(b) shows the sum of the flow to the internal (ICA) and external (ECA) carotid arteries, which is markedly different from the flow at the CCA (labelled as rigid wall). Instantaneous flows between the two consecutive PC slices along the CCA are also different. These changes in the flow waveforms are due to the compliance of the arterial walls, and cannot be neglected in the finite element modelling. It must be noted that although instantaneous flows do not add up to zero, the total flows over a cardiac cycle do. The two flow measurements along the CCA were used to derive the pressure waveform using a lumped parameter model. A fluid–structure interaction simulation was then carried out imposing Womersley velocity profiles at the exits from the ICA and ECA and traction-free boundary conditions at the entrance of the CCA with the reconstructed pressure waveform. The computed flow rate at the entrance of the CCA is also shown in Figure 3(b). Although this compliant model does not perfectly reproduce the measured flow at that location, it certainly represents a much better approximation than a rigid model.

E.3 *Thorax*: This last case is concerned with the air flow in the bronchii and lungs. The segmented image, together with the cuts at the extremities of the smaller branches, is shown in Figure 4(a). The mesh sizes were automatically obtained from an adaptive background grid with 6 levels of refinement. This produced the surface mesh shown in Figure 4(b). One can discern the smaller elements in regions of higher curvature and smaller vessel diameter. The volume mesh had approximately 1 million elements. In this first study, only the steady airflow was considered. The results obtained can be seen in Figures 4(c) and 4(d) which show surface pressures and iso-surfaces of constant absolute value of velocity.

 

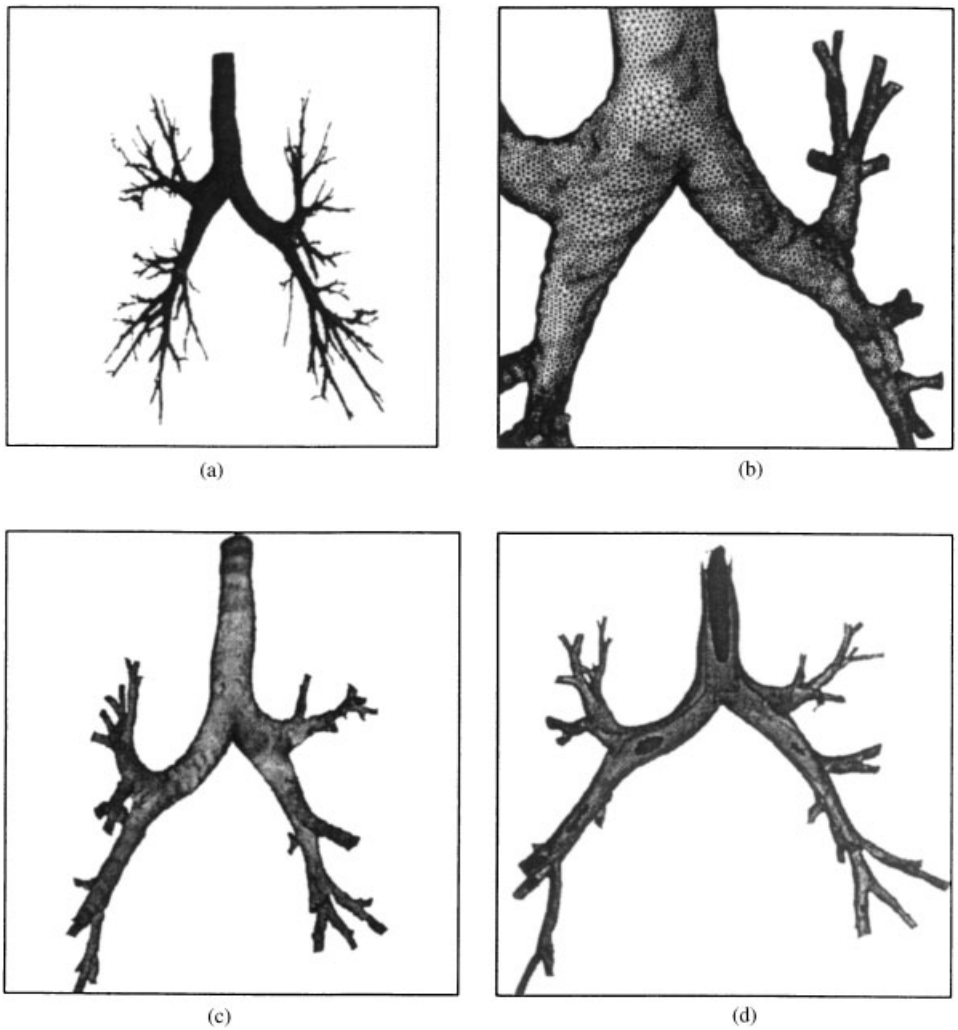


Figure 4. (a, b) Thorax: segmented image and surface mesh and (c, d) thorax: surface pressures and iso-surfaces of abs(velocity).

## 10. CONCLUSIONS AND OUTLOOK

The ability to predict accurately flows in the vascular and pulmonary system on a patient-specific basis has increased dramatically in the last years. We expect progress to continue in all the areas that encompass a comprehensive simulation capability: image segmentation, grid generation, flow solvers, fluid–structure interaction, data reduction and visualization. Some of the outstanding questions involve boundary conditions, material parameters (in particular for wall compliance), and the clinical significance of particular flow phenomena.

 

At present, image-based, patient-specific computational hemodynamics can be used to

- Study vascular diseases;
- Enhance diagnosis; and
- Plan surgical procedures.

Imaging modalities will continue to evolve and eventually both anatomy and physiology will be accurately visualized. However, the power of computer simulations lies in their ability to predict the outcome of procedures, i.e. the answer to 'what if' questions that can be useful for optimizing therapies. Looking into the more distance future, we foresee:

- CFD enhanced radiology;
- Simulations of long-terms effects, such as plaque formation;
- Simulations of drug delivery and effects; and
- The coupling of flow codes (continuum level) and particle codes (molecular level).

## REFERENCES

1. Barequet G, Shapiro D, Tal A. History consideration in reconstructing polyhedral surfaces from parallel slices. *Proceedings of the IEEE Visualization '96*, San Francisco, 1996; 149–156.
2. Quarteroni A, Tuveri M, Veneziani A. Computational vascular fluid dynamics: problems, models and methods. *Reports of EPFL/DMA* 11.98, 1998.
3. Taylor CA, Hughes TJR. Zarins CK. Finite element modeling of blood flow in arteries. *Computer Methods in Applied Mechanics and Engineering* 1998; **158**:155–196.
4. Moore JA, Steinman DA, Holdsworth DW, Ethier CR. Accuracy of computational hemodynamics in complex arterial geometries reconstructed from magnetic resonance imaging. *Annals of Biomedical Engineering* 1999; **27**:32–41.
5. Klette R, Zamperoni P. *Handbook of Image Processing Operators*. Wiley: New York, 1996.
6. Burdin V, Roux C. Surface segmentation of long bone structures from CT images using a deformable contour model. *Proceedings of 16th Annual International Conference on Engineering in Medicine and Biology*, November 3–6, Baltimore, 1994.
7. Vemuri BC, Guo Y, Lai SH, Leonard CM. Fast algorithms for fitting multiresolution hybrid shape models to brain MRI. *Lecture Notes in Computer Science*, vol. 1131. Springer: Berlin, 1996; 213–222.
8. Jones TN, Metaxas D. Automated 3D segmentation using deformable models and fuzzy affinity. *Lecture Notes in Computer Sciences*, vol. 1230. Springer: Berlin, 1997.
9. Lee CT, Kashyap RL, Chu CN. Building skeleton models via 3D medial surface/axis thinning algorithms. *Graphical Models and Image Processing* 1994; **56**:462–478.
10. Kawata Y, Niki N, Kumazaki T. Computer-assisted analysis and 3D visualization of blood vessels based on cone-bean CT images. *Lecture Notes in Computer Science*, vol. 1024. Springer: Berlin, 1995; 355–362.
11. Masutani Y, Masamune K, Dohi T. Region growing based feature detection algorithm for tree-like objects. *Lecture Notes in Computer Science*, vol. 1131. 1996; 161–172.
12. Wilson DL, Noble JA. Segmentation of cerebral vessels and aneurysms from MR agiographic data. *Lecture Notes in Computer Science*, vol. 1230. Springer: Berlin, 1997; 423–428.
13. Yim O, Summers RM. Analytic surface reconstruction by local threshold estimation in the case of simple intensity contrasts. *Proceedings of the SPIE Medical Imaging*, vol. 3660, 1999; 288–300.
14. Dale AM, Fischl B, Sereno MI. Cortical surface based analysis I: segmentation and surface reconstruction. *NeuroImage* 1999; **9**(2):179–194.
15. Cebral J, Löhner R. Advances in visualization: distribution and collaboration. *AIAA*-99-0693; 1999.
16. Cebral J, Löhner R. From medical images to CFD meshes. *Proceedings of the 8th International Meshing Roundtable*, South Lake Tahoe, October 1999.
17. Cebral JR, Löhner R. Automatic grid generation for anatomically accurate computational hemodynamics calculations. *Proceedings of the ICMMB-11*, April 2–5, Hawaii, 2000.
18. Cebral JR, Löhner R. Image-based computational hemodynamics. *Proceedings of the World Congress in Medical Physics and Biomedical Engineering*, Chicago, IL, July 23–28, 2000.
19. Cebral JR, Löhner R, Burgess J. Computer simulation of cerebral artery clipping: relevance to aneurysm neuro-surgery planning. *Proceedings of ECCOMAS 2000 Conference*, Barcelona, Spain, September, 2000.
20. Hoppe H, DeRose T, Duchamp T, McDonald J, Stuetzle W. Mesh Optimization. *SIGGRAPH 93 Proceedings*, 1993; 19–26.

 

21. Frey PJ, Borouchaki H. Surface mesh evaluation. *Proceedings of the 6th International Meshing Roundtable*, October 13–15, Park City, Utah, 1997.
22. Taubin G. A signal processing approach to fair surface design. *Computer Graphics Proceedings*, 1995; 351–358.
23. Cebral J, Löhner R. Flow visualization on unstructured grids using geometrical cuts, vortex detection and shock surfaces. *AIAA*-01-0915, 2001.
24. Cebral J, Cebral JR, Lohner R, Choyke PL, Yim PJ. Merging of intersecting triangulations for finite element modeling. *Journal of Biomechanics* 2001; **34**:815–819.
25. Löhner R. Regridding surface triangulations. *Journal of Computational Physics* 1996; 126:1–10.
26. Löhner R. Extensions and improvements of the advancing front grid generation technique. *Communications in Numerical Methods in Engineering* 1996; **12**:683–702.
27. Löhner R. Advances in unstructured grid generation. *Proceedings of the ECCOMAS 2000 Conference*, Barcelona, Spain, September, 2000.
28. Löhner R, Yang Chi, Cebral J, Soto O, Camelli F, Baum JD, Luo H, Mestreau E, Sharov D, Ramamurti R, Sandberg W, Oh Ch. Advances in FEFLO; *AIAA*-01-0592, 2001.
29. Taylor C, Hood P. A numerical solution of the Navier–Stokes equations using the finite element method. *Computers and Fluids* 1973; **1**:73–100.
30. Fortin M, Thomasset F. Mixed finite element methods for incompressible flow problems. *Journal of Computational Physics* 1979; **31**:113–145.
31. Franca LP, Hughes TJR, Loula AFD, Miranda I. A new family of stable elements for the Stokes problem based on a mixed Galerkin least-squares finite element formulation. In Chung TJ, Karr G (eds), *Proceedings of the 7th International Conference on Finite Elements in Flow Problems*, Huntsville, AL, 1989.
32. Franca LP, Frey SL. Stabilized finite element methods: II. The incompressible Navier–Stokes equations. *Computer Methods in Applied Mechanics and Engineering* 1992; **99**:209–233.
33. Tezduyar TE, Shih R, Mittal S, Ray SE. Incompressible flow computations with stabilized bilinear and linear equal-order interpolation velocity–pressure elements. *UMSI Report* 90, 1990.
34. Löhner R, Yang Chi, Oñate E, Idelssohn S. An unstructured grid-based, parallel free surface solver. *Applied Numerical Mathematics* 1999; **31**:271–293.
35. Wigton LB, Yu NJ, Young DP. GMRES acceleration of computational fluid dynamics codes. *AIAA*-85-1494-CP, 1985.
36. Saad Y, Schultz MH. GMRES: a generalized minimal residual algorithm for solving nonsymmetric linear systems. *SIAM Journal of Scientific and Statistical Computation* 1986; **7**(3):856–869.
37. Venkatakrishnan V. Newton solution of inviscid and viscous problems. *AIAA*-88-0413, 1988.
38. Saad Y. Krylov subspace methods on supercomputers. *SIAM Journal on Scientific and Statistical Computing* 1989; **10**(6):1200–1232.
39. Luo H, Baum JD, Löhner R. Edge-based finite element scheme for the Euler equations. *AIAA Journal* 1994; **32**(6):1183–1190.
40. Löhner R. Renumbering strategies for unstructured-grid solvers operating on shared-memory, Cache-based parallel machines. *Computer Methods in Applied Mechanics and Engineering* 1998; **163**:95–109.
41. Luo H, Baum JD, Löhner R. A fast matrix-free implicit method for compressible flows on unstructured grids. *Journal of Computational Physics* 1998; **146**:664–690.
42. Luo H, Baum JD, Löhner R. An Accurate, fast, matrix-free implicit method for computing unsteady flows on unstructured grids. *Computers and Fluids* 2001; **30**:137–159.
43. Mavriplis D. A unified multigrid solver for the Navier–Stokes equations on unstructured meshes. *AIAA*-95-1666, 1995.
44. Mavriplis D. A 3-D agglomeration multigrid solver for the Reynolds-averaged Navier–Stokes equations on unstructured meshes. *International Journal for Numerical Methods in Fluids* 1996; **23**:527–544.
45. Womersley JR. Method for the calculation of velocity. Rate of flow and viscous drag in arteries when the pressure gradient is known. *Journal of Physiology* 1955; **127**:553–563.
46. Perktold K, Rappitsch G. Computer simulation of arterial blood flow. Vessels diseases under the aspect of local hemodynamics. In Jaffrin MY, Caro C. (eds). *In Biological Flows*. Plenum Press: New york, 1995, 83–114.
47. Zhao SZ, Xu XY, Hughes AD, Thom SA, Stanton AV, Ariff B, Long Q. Blood flow and vessel mechanics in a physiologically realistic model of a human carotid arterial bifurcation. *Journal of Biomechanics* 2000; **33**: 975–984.
48. Ladak HM, Thomas JB, Mitchell JR, Rutt BK. Steinman DA. A semi-automatic technique for measurement of arterial wall from black blood MRI. *Medical Physics* 2002; **28**(6):1098–1107.
49. Baum JD, Luo H, Löhner R, Yang C, Pelessone D, Charman C. A coupled fluid/structure modeling of shock interaction with a truck. AIAA-96-0795, 1996.
50. Löhner R. Robust, vectorized search algorithms for interpolation on unstructured grids. *Journal of Computational Physics* 1995; **118**:380–387.
51. Maman N, Farhat C. Matching fluid and structure meshes for aeroelastic computations: a parallel approach. *Computers and Structures* 1995; **54**(4):779–785.

 

52. Cebral JR, Löhner R. Conservative load projection and tracking for fluid–structure problems. *AIAA Journal* 1997a; **35**(4):687–692.
53. Cebral JR, Löhner R. Fluid–Structure coupling: extensions and improvements. *AIAA*-97-0858; 1997b.
54. Lesoinne M, Farhat Ch. Geometric conservation laws for flow problems with moving boundaries and deformable meshes, and their impact on aeroelastic computations. *Computer Methods in Applied Mechanics and Engineering* 1996; **134**:71–90.
55. Yim PJ, Mullick R, Summers RM, Marcos H, Cebral JR, Löhner R, Choyke PL. Measurement of stenosis from Magnetic resonance angiography using vessel skeletons. *Proceedings of SPIE*, vol. 3978, 2000; 245–255.

 